Volume 1 | Number 1 | Jan 2013 | Pages 1–100

Journal of
Materials Chemistry C

Materials for optical and electronic devices
www.rsc.org/materialsC

ROYAL SOCIETY
OF CHEMISTRY

ROYAL SOCIETY
OF CHEMISTRY

www.rsc.org/materialsC

Fabrication of novel nanoscale *salt* utilized as substrates for the formation of gold-shelled composite nanomaterials.

Journal Name

ARTICLE

Soft- and Hard-Templated Organic Salt Nanoparticles with the Midas Touch: Gold-Shelled NanoGUMBOS

A.R. Wright,[†] M. Li,[†,‡] S. Ravula,[‡] M. Cadigan,[¥,§] B. El-Zahab,[†,∥] S. Das,[†] G.A. Baker,[*,‡] and I.M. Warner[*,†]

An emerging thrust in the design of advanced materials is nanoscale functional materials possessing multiple capabilities, such as those possessing a core–shell architecture. Nanoparticles comprising a dielectric core (e.g., silica, polystyrene) and a gold shell are particularly attractive due to the desirable optical (plasmonic) and biocompatibility characteristics of gold. While these materials are bio-inert, they generally present limited tunability. In this regard, a core composed of a solid-state ionic liquid represents an interesting and unexplored alternative for generating unique core–shell architectures. In recent years, we have developed an emergent class of morphology-controlled tailored organic salt particles, so-called GUMBOS (group of materials based on organic salts). GUMBOS are reminiscent of traditional ionic liquids with the important distinction that they possess elevated melting points (generally, from 100 to 250 °C), making possible the fabrication of ambient-stable nanoscale salts of various sizes, compositions, and morphologies by means of a variety of thermal, sonochemical, colloidal, or hard-template synthetic routes. In this work, we advance our recent examination of GUMBOS to demonstrate proof of concept for their use in elaborating novel plasmonic nanostructures by using a seed-mediated growth to generate gold shells atop nanoscale quasi-spherical GUMBOS as well as uni-dimensional GUMBOS nanorods. We present here our general strategy for preparing gold-shelled nanoGUMBOS, alongside systematic monitoring of the evolution of the gold-coating process. We also report on a preliminary investigation of the catalytic properties of the near-infrared absorbing gold-shelled nanorod GUMBOS in the reduction of 4-nitrophenol to 4-aminophenol using sodium borohydride.

Introduction

Core–shell nanostructures consisting of an inner "core" material surrounded by an external "shell" layer of a different material represent a nanoscale morphology of growing interest. These materials vary widely and can consist of organic/organic, organic/inorganic, inorganic/organic, or inorganic/inorganic core–shell combinations.[1] In many cases, gold is used as the outer layer due to its useful optical, catalytic, electronic, inert, biocompatible, and functional properties. The concept of gold-coated nanoparticles was pioneered by Oldenburg et al. in 1998.[2] These authors reported a preparation technique for systematically depositing variable-thickness gold nanoshells onto monodispersed silica-cored nanoparticles. The absorption and scattering properties of these nanoparticles were tunable based on the core size relative to the nanoshell thickness. Higher core : shell ratios resulted in higher absorption in the near infrared (NIR) region of the electromagnetic spectrum. This extended absorption profile for gold as a thin layer surrounding a dielectric core was unprecedented since the absorption of traditional gold nanoparticles is limited to the visible region of the electromagnetic spectrum. Following this initial report by Oldenburg et al.,[2] subsequent composite nanoparticles using different core–shell combinations such as silica–silver,[3] silica–gold/silver alloy,[3] polystyrene–gold,[4] and polystyrene–silver[4] were reported. The NIR absorption of these gold-coated core–shell nanoparticles initiated investigations of these composite nanomaterials for cancer cell imaging and photothermal therapy since NIR irradiation can harmlessly penetrate skin and sub-dermal tissues.[5] The photothermal

applications of gold stem from its strong absorption cross section as well as its ability to transform optical irradiation into heat to generate localized hyperthermia.[6,7] That is, when tumor-targeted gold nanoshells accumulate with cancer cells, introduction of NIR laser light induces a temperature increase within the cell. An increase of 30–35 °C is considered significant enough to result in cellular death.[8] This photothermal therapy is non-invasive and can in principle be made specific for cancerous cells, leaving healthy tissues unaffected.[9]

The properties of nanomaterials depend strongly upon their morphology (i.e., size and shape). For instance, one-dimensional (1-D) gold nanorods exhibit different optoelectronic properties than their spherical counterparts. Indeed, gold nanorods display two plasmon resonances, a transverse band located near 520 nm which is representative of the absorption across the diameter of the nanorod and a longitudinal band appearing in the 600–1600 nm regime which corresponds to absorption along the length of the nanorod. This latter plasmon band is dependent on the aspect ratio of the nanorod.[10] The ability of nanorods to absorb and scatter in the NIR region of the electromagnetic spectrum makes them attractive contrast agents with promise in photothermal therapy.[11]

An emergent class of task-specific salts referred to as groups of uniform materials based on organic salts (GUMBOS), offers multiple levels of tailorability, making them fitting for a range of applications. GUMBOS are an extension of traditional ionic liquids (ILs) and offer many of the attractive properties attributed to ILs. In contrast to ILs, however, GUMBOS are designed to remain solid at their operation temperature, with typical melting points in the 25 to 250 °C range, thus expanding on the library of functional materials that can be prepared. This simple but powerfully general idea has expanded into the field of nanoscience and the tailoring of nanoscale GUMBOS (hereafter, nanoGUMBOS), which represent nanomaterials derived from modestly high-melting (super-ambient) organic salts. Already, nanoGUMBOS have been shown to exhibit unique properties (optical, for example) that do not exist within the bulk material.[12,13,14] Taking advantage of the easy functionalization, tunability, and attractive properties of nanoGUMBOS and gold nanomaterials, we report here on a general route to obtain core–shell nanostructures comprising a gold shell surrounding a nanoGUMBOS salt core. Initially, spherical nanoparticles of 1-methyl-3-propylimidazolium bis(trifluoromethylsulfonyl)imide [MImProSH][NTf$_2$] were prepared using a reverse micelle nanoreactor approach, as described earlier by Tesfai et al.[12] Nanorods consisting of [MImProSH][TPB] (TPB = tetraphenylborate) were prepared following a hard-template route developed by de Rooy et al.[15] The growth and spectral properties of the gold-shelled nanoGUMBOS were examined and a preliminary investigation of their behavior for the catalytic reduction of 4-nitrophenol to 4-aminophenol by sodium borohydride is undertaken in this work.

Results and discussion

Morphological and Optical Properties of GUMBOS and NanoGUMBOS

The GUMBOS materials used in the construction of nanoparticles were prepared using a two-step synthesis scheme involving alkylation followed by metathesis with the desired anion. The physical properties of GUMBOS can be effectively tuned by the cation and anion combination employed. Essentially spherical GUMBOS nanoparticles as well as 1-D nanorods were correspondingly prepared from two different GUMBOS salts selected for their particular hydrophobic characteristics. In particular, [TPB]$^-$ salts possess a somewhat higher hydrophobicity than those of [NTf$_2$]$^-$ while also affording a higher melting temperature, making [TPB]$^-$ salts more appropriate to the AAO solid template route for elaborating nanorods. Shown in Fig. 1 is the absorption profile for [MImProSH][NTf$_2$] dissolved in acetone, displayed alongside the spectrum of an aqueous suspension of [MImProSH][NTf$_2$]-derived nanoGUMBOS formed by the reverse micelle templating strategy displayed earlier in Fig. 1. Despite being composed of the same ionic parent material, the GUMBOS starting material shows a sharp absorption maximum at 209 nm, whereas the absorbance for the nanoscale material is significantly broadened and bathochromically shifted to 265 nm.
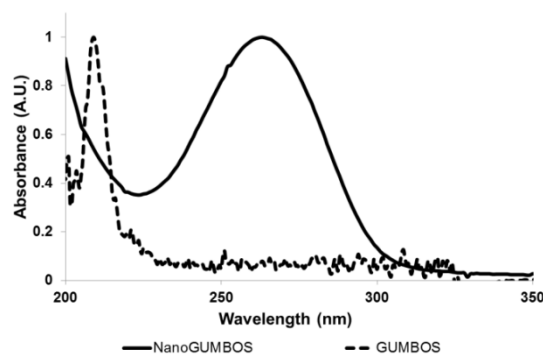
Fig. 1 UV–Vis absorption spectrum of bulk [MImProSH][NTf$_2$] GUMBOS dissolved in acetone and the corresponding nanoGUMBOS colloids dispersed in water.

The use of the reverse micelle method for preparation of nanoGUMBOS has been described previously by Tesfai et al.[12] Elucidated in this report is the direct relationship between reactant concentration and the size and monodispersity of the resulting nanoGUMBOS. Under the conditions described in the experimental section, nanoGUMBOS possessing an average diameter of 157 ± 47 nm were formed, as shown in Fig. 2A. In agreement with our earlier observations, the size of the nanoGUMBOS can be easily controlled by adjusting the initial concentrations of the parent compounds [MImProSH]Cl and Li[NTf$_2$]. For example, reducing the reactant concentrations three-fold to 1.0 M yielded nanoGUMBOS with an average diameter of 21 ± 5 nm (Fig. 2B). In general, the use of lower

reactant concentrations reduces the polydispersity slightly (relative standard deviation (RSD) values of 24% and 30% were determined for 1.0 M and 3.0 M starting concentrations, respectively) as well as the population density of the resulting nanoGUMBOS, as can be observed by comparing the two micrographs of Fig. 2. This same trend in concentration-dependent polydispersity was noted previously during our reverse micellar route to $[Bm_2Im][BF_4]$ and $[Bm_2Im][FeCl_4]$ nanoGUMBOS. In that work, we attributed these observations to the higher diffusion collision and ion exchange rates of reactants present at higher concentrations which shift the coalescence/decoalescence equilibrium during nanoparticle synthesis.[12]
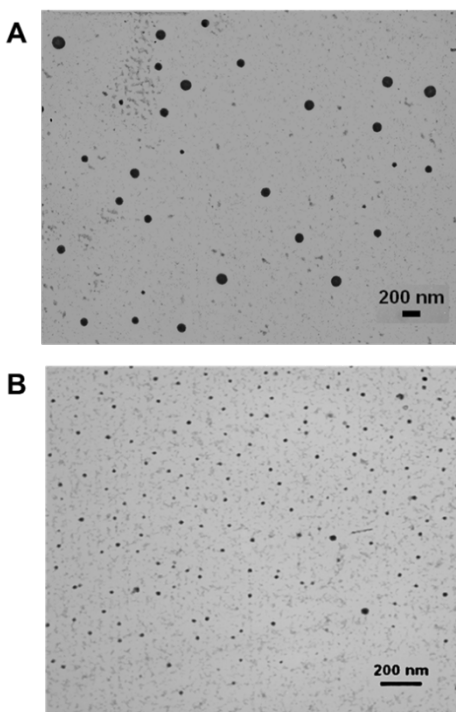
Fig. 2 Representative TEM micrographs of thiol-functionalized $[MImProSH][NTf_2]$ nanoGUMBOS prepared using a reverse micelle templating route. Shown are nanoGUMBOS with average diameters of (A) 157 ± 47 nm and (B) 21 ± 5 nm formed from 3.0 M and 1.0 M preparatory aqueous-phase concentrations of the parent ions, respectively.

Gold Nanoshell Formation

Gold nanoshell formation was prefaced by the attachment of tiny (~5 nm) gold seeds onto the surfaces of $[MImProSH][NTf_2]$ nanoGUMBOS. The thiols present at the nanoGUMBOS surface aid in the covalent fixation of gold seeds which then serve as immobilized nucleation sites for the catalytic growth of the gold nanoshell. Fig. 3 shows a typical TEM micrograph of the gold seeds and a corresponding UV–Vis absorbance spectrum of the gold seeds before and after attachment to the $[MImProSH][NTf_2]$ nanoGUMBOS. The absorbance spectrum of an aqueous solution of gold seeds reveals a shoulder near 510 nm, but does not show a well-

defined localized surface plasmon resonance (LSPR) band typical of larger gold nanoparticles. Indeed, behavior of this sort is often observed with gold nanoparticles having diameters well below 10 nm.[16,17] Once the gold seeds become fixed to the nanoGUMBOS, an LSPR band becomes evident, as can be witnessed in the magnified view of the spectrum. This result is attributed to a partial aggregation of gold seeds on the surface of the nanoGUMBOS.[3] In particular, an LSPR band at 513 nm is consistent with 5 nm gold seeds becoming adsorbed on the surface of a non-metallic core nanoparticle.[3,4,18]

The final nanoshell morphology and the corresponding optical behavior is highly dependent on the volumetric ratio between the gold hydroxide solution to the gold-seeded nanoGUMBOS, in accord with previous results reported in the literature.[2,4] A range of different gold hydroxide solution to gold-seeded nanoGUMBOS ratios were investigated for both concentrations of $[MImProSH][NTf_2]$ nanoGUMBOS. Figs. 4A and 4B provides the UV–Vis absorption profiles resulting from employing 1:1, 2:1, 4:1, 8:1, 20:1, and 40:1 ratios of gold hydroxide to 157 nm gold-seeded nanoGUMBOS. Fig. 4C is a display of the corresponding TEM micrographs, which clearly illustrate some key aspects of the nanoshell growth and maturation process. In the presence of gold hydroxide solution and the "mild" reducing agent formaldehyde, the seeds adsorbed onto the surface grow and coalesce with adjacent seeds until a partial monolayer of gold covers the nanoGUMBOS. As the amount of gold hydroxide increases, additional gold from the growth solution begins to fill the voids until a complete monolayer is formed.
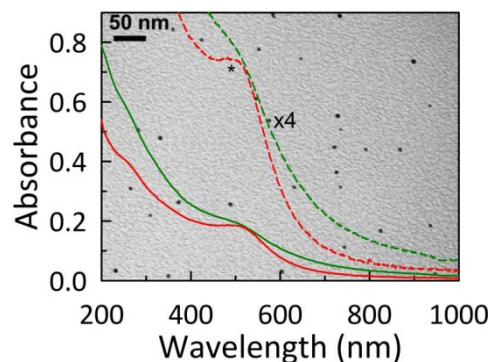
Fig. 3 Absorption spectra of gold seeds before (green profile) and after (red spectrum) attachment to $[MImProSH][NTf_2]$ nanoGUMBOS. A representative TEM micrograph of the tiny gold seeds provides the backdrop image in this figure.

Spectroscopically, the absorption maxima continuously shift to longer wavelengths and broaden as gold fills the voids on the core surface until complete coverage is achieved. As the nanoshell becomes thicker, the LSPR begins to shift to lower wavelengths. In the case of the 157 nm nanoGUMBOS (core), the absorbance maxima observed are 619, 679, 757, 874, 773, and 715 nm for gold hydroxide : gold-seeded nanoGUMBOS ratios of 1:1, 2:1, 4:1, 8:1, 20:1, and 40:1, respectively. This suggests that nanoshells are completely formed at an 8:1 ratio of gold hydroxide to 157 nm gold-seeded nanoGUMBOS, in this case. Notably, the absorbance profile for the 8:1 ratio

exhibits a pronounced broad peak from 900 to 1100 nm not seen for the other ratios. The TEM micrographs in Fig. 4C depict the completion of the nanoshell growth in proceeding from a gold hydroxide : gold-seeded nanoGUMBOS ratio of 1:1 to 8:1. The images are in excellent agreement with the optical data, showing an increased gold coverage as the ratios increase with complete nanoshells formed at a ratio of 8:1.
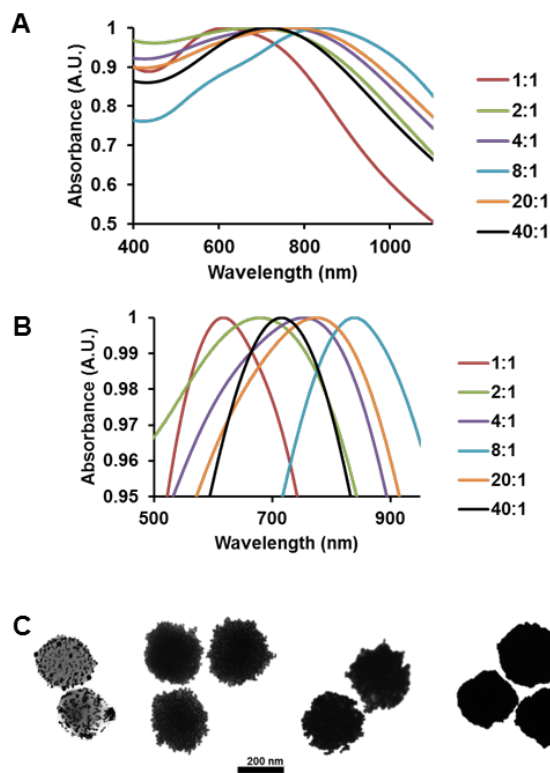
Fig. 4 (A) Normalized UV–Vis absorption spectra tracking the growth of (i) gold nanoshells on 157 ± 17 nm nanoGUMBOS based on [MImProSH][NTf$_2$]. Panel (B) shows the magnified absorption maxima. (C) Evolution of gold nanoshell morphology with increasing ratios of gold hydroxide solution to gold-seeded nanoGUMBOS (i) 1:1, (ii) 2:1, (iii) 4:1, and (iv) 8:1.

The absorption profiles and associated TEM images for gold shell growth on 21 nm nanoGUMBOS cores are presented in Fig. 5. For this smaller core unit, as the ratio of gold hydroxide solution to nanoGUMBOS was increased in the order 1:1, 2:1, 4:1, 8:1, and 20:1, the absorbance maxima recorded were 715, 813, 774, 759, and 733 nm, respectively. These results indicate that nanoshell formation was complete at the 2:1 ratio. Conspicuously, the LSPR maximum for nanoshell completion on the smaller core nanoGUMBOS occurred some 61 nm lower in wavelength than for the larger core size. Korgel and co-workers have recently investigated the limitations on the optical tunability of gold nanoshells grown on various silica nanoparticle core sizes, determining that the tunability in the LSPR maximum for smaller-diameter nanoshells suffers due to a reduced range of accessible core−shell ratios as the core diameter shrinks.[18] Indeed, the core-to-shell ratio determines the absorbance plasmon peak; thus, restricting the maxima to lower wavelengths for smaller

core sizes. TEM images for the 1:1 and 2:1 ratios display an agglomeration of nanoGUMBOS particles not seen in experiments with larger core sized nanoGUMBOS. An increased agglomeration of gold was witnessed for the higher ratios. This general observation was pointed out by the Korgel group for gold nanoshell growth on silica nanoparticles.[18] That is, smaller diameter nanoshells were found to be highly prone to aggregation (broadening the plasmon absorption peak), possibly due to the size-dependence of the electrostatic double-layer potential.
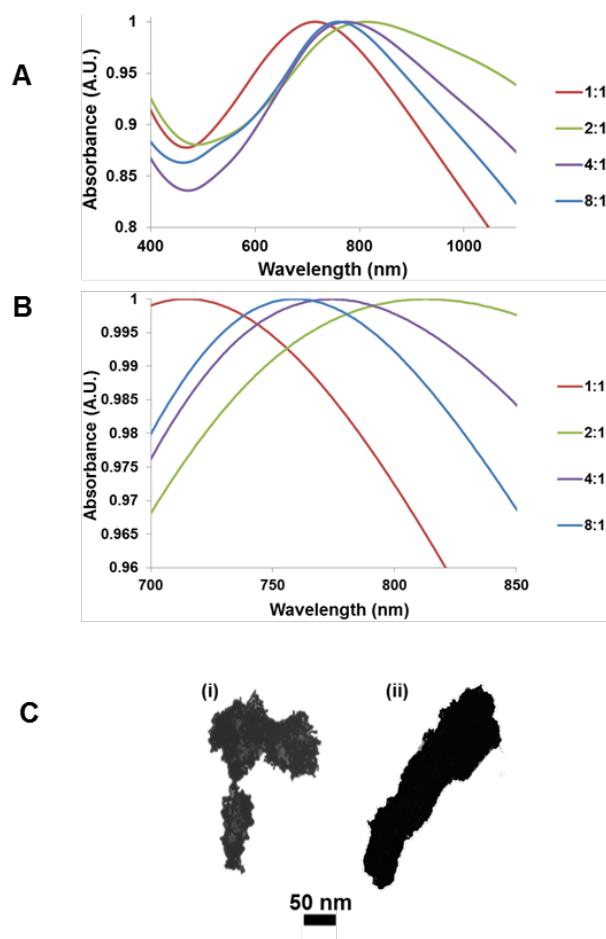
Fig. 5 Normalized UV–Vis spectra of gold nanoshell growth on (A) 21 ± 5 nm nanoGUMBOS based on [MImProSH][NTf$_2$] alongside (B) an expanded view of the absorption maxima. (C) TEM micrographs for nanoshell progression on gold-seeded nanoGUMBOS for gold hydroxide solution to gold-seeded nanoGUMBOS ratios of (i) 1:1 and (ii) 2:1.

Morphological and Optical Characterization of 1-D NanoGUMBOS

Fig. 6 is a display of SEM micrographs of 1-D nanoGUMBOS prepared from [MImProSH][TPB] GUMBOS using an AAO template. The resulting nanorods have narrowly-dispersed diameters in the 240 to 280 nm range. These diameters are noticeably larger than the claimed 200 nm pore size of the AAO discs used as templates. A recent report observed a similar swelling behavior for nanorods after removal from the AAO template.[15] The evolution of core–shell 1-D

nanoGUMBOS built around [MImProSH][TPB] as a core material is displayed in Fig. 7. Gold-seeded nanorods (Fig. 7B) were obtained after 48 h of immersion in gold seed solution. Shown in Fig. 7C are illustrative gold-coated rod-shaped [MImProSH][TPB] nanoGUMBOS.
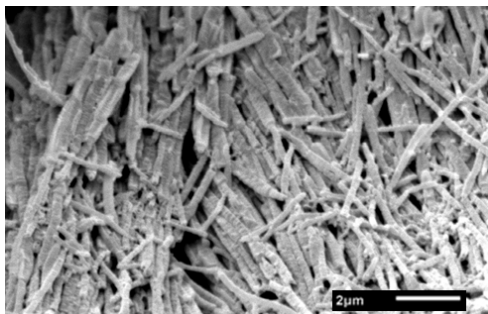
Fig. 6 SEM micrographs of nanoGUMBOS rods based on [MImProSH][TPB].
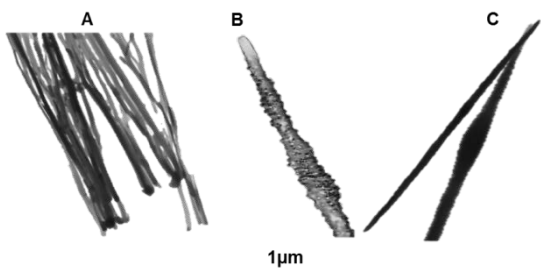
Fig. 7 Representative TEM micrographs of (A) bare [MImProSH][TPB] rods, (B) gold-seeded [MImProSH][TPB] rods, and (C) gold-shelled 1-D [MImProSH][TPB] nanoGUMBOS rods.
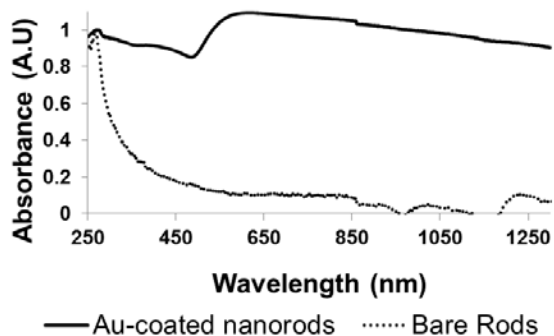
Fig. 8 Absorption/extinction spectra of bare 1-D [MImProSH][TPB] nanoGUMBOS (dotted trace) and the corresponding gold-shelled [MImProSH][TPB] nanoGUMBOS rods (solid profile).

Fig. 8 compares the optical responses of bare [MImProSH][TPB] nanorods with their gold-coated counterparts. The common peak at 265 nm represents bare [MImProSH][TPB] nanorods suspended in an aqueous medium. There is a dramatic increase in absorption for gold-coated nanorods across the entire visible spectrum and well into the NIR (the upper wavelength represents the limitation of our

spectrometer). To our knowledge, there are no previous reports of such intense "panchromic" absorption for alternate gold-coated nanorods, organic or otherwise, suggesting intriguing potential for these materials in a variety of areas.

Catalytic Reduction of 4-Nitrophenol by Gold-Shelled GUMBOS

The reduction of 4-nitrophenol (4-NP) to 4-aminophenol (4-AP) was chosen as a benchmark reaction to evaluate the catalytic activity of gold-shelled nanoGUMBOS because this model reaction has been well-studied over the past decade and can be conveniently monitored by use of UV–Vis spectroscopy.[19,20,21] In this work, the catalytic activity of the GUMBOS nanorods was determined at room temperature in a large excess of $NaBH_4$, conditions ensuring pseudo-first-order conditions would be operative with respect to 4-NP. In a typical experiment, 3.4 mM of 4-NP was combined with a large excess of $NaBH_4$ (150 mM) in the absence or presence of catalyst. As shown in Fig. 9A, 4-NP in water has an absorbance peak centered around 320 nm. Addition of $NaBH_4$ to 4-NP brings about a red shift to 400 nm and a dramatic increase in absorbance (hyperchromicity) due to deprotonation of 4-NP to produce the 4-nitrophenolate ion. Whereas the uncatalyzed reaction showed no progress, under identical conditions the gold-shelled GUMBOS nanorods induced a rapid fading of the yellow color of 4-NP within a few minutes. Indeed, in the absence of catalyst (i.e., in the presence of $NaBH_4$ alone), the absorbance peak at 400 nm remained unaltered even after 100 min, indicating a complete lack of reaction on this timescale; see Fig. 9B. In contrast, in the presence of the gold-shelled GUMBOS nanocatalyst, reduction of 4-NP to 4-AP was observed by the rapid loss of the 400 nm peak with attendant appearance and growth of a new peak at 300 nm attributable to 4-AP (Fig. 9C).

Interestingly, in the presence of the gold-shelled GUMBOS catalyst, no reduction of 4-NP initially took place until 600 s. Such an induction time (t_0; Fig. 9D) prior to 4-NP reduction has been observed previously for a number of different carrier systems.[22] The primary role of the catalyst is to facilitate electron transfer from borohydride ion to the 4-nitrophenolate ion at the nanoparticle surface.[23] The induction period has been attributed to a slow, spontaneous reconstruction of the nanoparticle surface, either as a shift of single atoms or perhaps a concerted rearrangement of multiple surface atoms. Sometimes, such reactions are explained in terms of the Langmuir–Hinshelwood mechanistic model in which the nanoparticle surface reacts with borohydride ions to form metal hydride, fast Langmuir isotherm (reversible) sorptions of 4-NP and $NaBH_4$ occur, and the rate-determining step entails the reduction of adsorbed 4-NP to 4-AP which subsequently detaches to free up the nanoparticle surface for another catalytic cycle.

As shown in Fig. 9D, after the induction period, loss of the 400 nm peak is very rapid and within several minutes, there is a total extinction of this peak, indicating complete conversion to

4-AP. Fig. 9D shows the linear relation between $\ln(A/A_0)$ and reduction time (after t_0), where A_0 is the absorbance at 400 nm at time zero. Such a linear correlation is consistent with a reaction first order in the concentration of 4-NP, a consequence of the excess of borohydride used. That is, the large amount of borohydride employed relative to 4-NP makes the concentration of $NaBH_4$ essentially constant during the reaction and allows pseudo-first-order kinetics to be used to evaluate the catalytic rate. From the linear portion of this plot, we can determine an apparent rate constant (k_{app}) for this reaction of 7.34×10^{-3} s^{-1}, a value found to be quite high compared to published values for known gold catalysts.
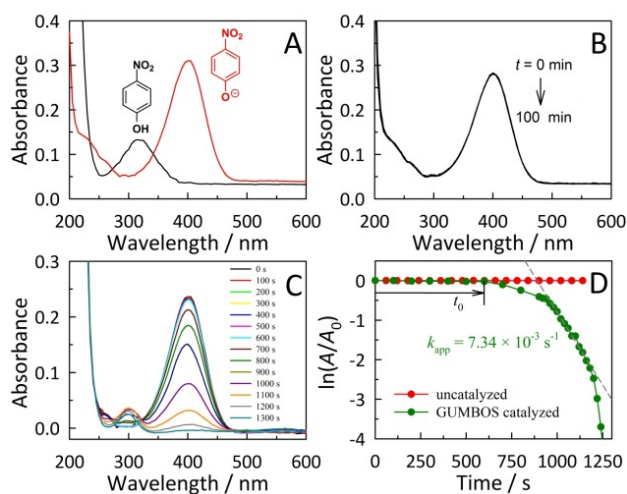
Fig. 9 UV–Vis absorption studies of the catalytic reduction of 4-nitrophenol by $NaBH_4$ in the presence of gold-shelled rod-shaped [MImProSH][TPB] nanoGUMBOS. (A) Absorption spectra of 4-nitrophenol in water and 4-nitrophenolate formed immediately after the addition of $NaBH_4$. (B) The reaction profile of 4-NP in the absence of catalyst showing negligible conversion after 100 min. (C) Successive spectra showing the reduction of 4-NP in the presence of excess $NaBH_4$ in aqueous media over gold-shelled nanorod catalyst over the course of 1300 s. (D) Plot of $\ln(A/A_0)$ *versus* time for the kinetic study of the reaction between 4-NP and $NaBH_4$. An induction time, t_0, is strikingly apparent for the catalyzed reaction. Absorbance (A) was monitored at 400 nm. The apparent rate constant, k_{app}, is taken from the slope of the linear region designated by the dashed grey line.

Experimental

Chemicals and reagents

Reagents were procured in the highest purities available and used as received. Lithium bis(trifluoromethylsulfonyl)imide (Li[NTf$_2$]), sodium tetraphenylborate (Na[TPB]), potassium carbonate (K$_2$CO$_3$), sodium hydroxide (NaOH), 1-methylimidazole, tetrakis(hydroxymethyl)phosphonium chloride (THPC, 80% in water), acetone, formaldehyde (37

wt% solution in water), isopropyl alcohol (IPA), cyclohexane, Triton X-100, 3-chloro-1-propanethiol, hydrogen tetrachloroaurate trihydrate (HAuCl$_4$), 4-nitrophenol (4-NP), and sodium borohydride were obtained from Sigma-Aldrich (St. Louis, MO, USA). Anodic aluminum oxide (AAO) membranes (13 mm disc diameter, 20 µm thickness, 200 nm pore sizes) manufactured by Whatman were purchased from SPI Supplies and Structure Probe, Inc. (West Chester, PA). Ultrapure water (18.2 MΩ cm) was obtained using an Elga model PURELAB Ultra water filtration system.

Synthesis of GUMBOS and NanoGUMBOS

The preparation of thiol-functionalized GUMBOS involved an alkylation reaction followed by anion metathesis. A 1:1 molar ratio of 1-methylimidazole and 3-chloro-1-propane thiol was mixed and purged under argon in the presence of approximately 15 mL of IPA for approximately 20 min. The solution was then refluxed at 80 °C for 48 h. Once the solution had completely cooled, the solvent was removed under vacuum to leave a slightly yellow, hygroscopic residue. The resulting salt [MImProSH]Cl was purified by washing with ethyl acetate in triplicate and then dried under vacuum. Anion metathesis and formation of nanoGUMBOS was accomplished simultaneously using a reverse micelle nanoreactors method outlined in Fig. 10. Initially, two separate 8 mL solutions of 0.4 M Triton X-100 were prepared in cyclohexane. Next, two separate solutions of 3.0 M [MImProSH]Cl and 3.0 M Li[NTf$_2$] were prepared in ultrapure water. A 40 µL aliquot of aqueous [MImProSH]Cl solution was added to one of the 8 mL Triton X-100 in cyclohexane solutions. A 40 µL aliquot of aqueous Li[NTf$_2$] was similarly added to the other Triton X-100 in cyclohexane solution. These separate reverse micelle solutions were each stirred for approximately 10 min. The two solutions were then gently combined and stirred for 18 h at room temperature. The resulting nanoGUMBOS suspension was centrifuged at 3200 rpm for 10 min and washed twice with cyclohexane, followed by a duplicate rinse with ultrapure water. Finally, the nanoGUMBOS were redispersed in 5 mL of deionized water for further characterization and study. NanoGUMBOS of smaller diameters are available from this general strategy by using lower original concentrations of [MImProSH]Cl and Li[NTf$_2$] in the initial reverse micelle stocks.
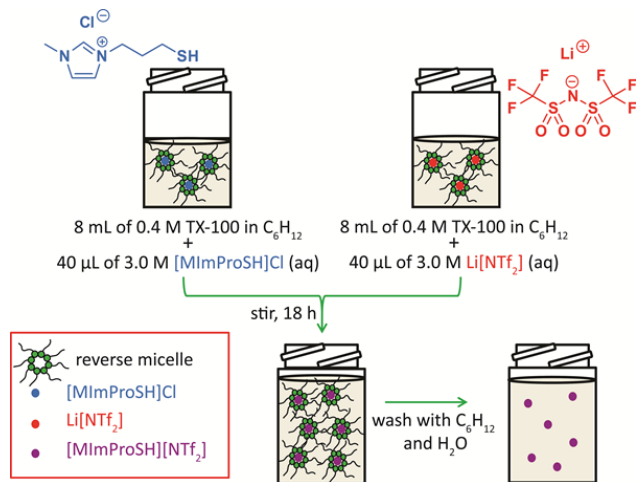
Fig. 10 Schematic diagram summarizing the reverse micelle nanoreactor strategy used in the preparation of [MImProSH][NTf$_2$] nanoGUMBOS.

Synthesis of Gold Seeds and Attachment to NanoGUMBOS Cores

Gold seeds of approximately 2–3 nm in diameter were prepared using a modification of a method previously reported by Duff et al.,[16,17] based on the reduction of HAuCl$_4$ with THPC. A 1.0 mL aliquot of NaOH (0.06 mmol), 2 mL of THPC solution (24 μL of THPC in 2 mL of water), and 200 mL of deionized water were stirred in a 250 mL volumetric flask for 15 min. A 4 mL aliquot of 1% (w/v) aqueous HAuCl$_4$ solution was added to the mixture and constantly stirred for an additional 30 min. The color of the reaction mixture immediately changed from colorless to a dark reddish-yellow. The solution was aged for at least three days at 4 °C before further use. After appropriate aging, the gold colloid seeds were contained in a brown solution. Attachment of the gold seeds was performed by stirring 1 mL of nanoGUMBOS solution with 5 mL of aged gold seeds for two days. The mixture was centrifuged three times and resuspended in fresh water.

Preparation of Gold-Nanoshelled NanoGUMBOS

Fig. 11 Progression in the appearance of samples resulting from the growth of gold shells atop 157 nm [MImProSH][NTf$_2$] nanoGUMBOS achieved using increasing volumetric ratios of gold hydroxide solution to gold-seeded nanoGUMBOS solution. The formation of a complete and relatively smooth gold nanoshell was attained at an 8:1 ratio.

Gold nanoshells were prepared following methods previously described by Kim et al. wherein a gold hydroxide solution was prepared by dissolving 0.05 g of K$_2$CO$_3$ in 200 mL of water and adding a 4 mL of 1% (w/w) HAuCl$_4$. The color of the mixture changed from yellow to colorless within 40 min. The solution was then aged for one day. Varying volumetric ratios of gold hydroxide to gold-seeded nanoGUMBOS solutions were then mixed. After 10 min, 0.025 mL of formaldehyde was added. Depending on the shell thickness, the color of the solutions ranged from translucent to dark blue after approximately 40 min (see Fig. 11). The nanoshells so formed were collected by centrifugation and then resuspended in water.

Preparation of 1-D NanoGUMBOS

Bulk GUMBOS material containing the tetraphenylborate anion were prepared by anion metathesis of [MImProSH]Cl with sodium tetraphenylborate (Na[TPB]). To begin, the two salts were individually dissolved in deionized water in appropriate amounts to yield a 1 : 1.1 molar ratio of [MImProSH]Cl to Na[TPB]. The two solutions were combined to immediately yield [MImProSH][TPB] as a white precipitate. Sodium chloride by-product was removed from the desired hydrophobic GUMBOS salt by deionized water washes performed in triplicate.

High-aspect 1-D nanoGUMBOS were generated from the prepared GUMBOS using a previously reported hard template method.[15] In brief, a saturated acetone solution of [MImProSH][TPB] was drop cast onto a Whatman anodic aluminum oxide (AAO) anodisc membrane-supported filter ~20 times, allowing each drop to dry fully before the next addition. The modified AAO disc was placed in an uncapped vial which was then nested within a beaker containing a small volume of acetone and the beaker sealed with inert plastic film. The beaker was placed in an oil bath held at 60 °C where it remained for 1 h. This process allowed acetone vapors to ensure complete coverage of the GUMBOS material within the AAO pores. Following this solvent annealing step, excess [MImProSH][TPB] was removed using 180-grit fine sandpaper. Free 1-D nanoGUMBOS were liberated by dissolving the AAO disc in 1 mM phosphoric acid solution overnight, followed by several deionized water flushes. The resulting GUMBOS nanorods were dried under vacuum overnight. Nanorod arrays were captured by adhering an AAO disk to a SEM stub prior to disk dissolution in preparation for SEM imaging.

Preparing Core–Shell 1-D NanoGUMBOS

The overall procedure for imparting gold nanoshell coatings to 1-D nanoGUMBOS is essentially the same as the approach described above for gold nanoshells grown on spherical nanoGUMBOS. Following the dissolution of the AAO disc used to template the growth of nanoGUMBOS rods, a solution of gold seeds was added to the freed nanoGUMBOS, followed by stirring for 48 h. Gold-seeded 1-D nanoGUMBOS were centrifuged and resuspended in 5 mL of water. A 1 mL aliquot of seeded rods was then added to 5 mL of gold hydroxide solution. After 5 min of stirring, 25 μL of formaldehyde was added, inducing a color change to an iridescent blue hue.

Catalytic Reduction of 4-Nitrophenol by Gold-Shelled GUMBOS

In a typical experiment to test the catalytic activity of gold-shelled nanorod-shaped GUMBOS, 200 μL of aqueous 4-nitrophenol (4-NP) solution (17 mM) were combined with 150

μL of freshly-prepared aqueous $NaBH_4$ (1.0 M) in a semi-micro (1.4 mL) Spectrosil® quartz optical cuvette (Starna Cells Inc., Atascadero, CA) to yield a deep yellow solution. To initiate reaction, 650 μL of as-prepared GUMBOS catalyst were injected into the above solution with careful mixing by gentle shaking to avoid bubble formation. The absorbance of the 4-nitrophenolate band at 400 nm was monitored over time using a Varian Cary Bio 50 UV–Vis spectrophotometer until a colorless solution was achieved, signifying completion of the reaction. A control experiment was performed in parallel by injecting an equivalent volume of water instead of catalyst solution, all other parameters remaining identical. Reactions were conducted at 298 K.

Characterization Techniques

The GUMBOS were characterized using NMR spectroscopy in d_6-DMSO on a Bruker DPX-250 MHz instrument. General absorption analyses were measured in aqueous solution at room temperature using a Perkin Elmer LAMBDA 750 UV–Vis–NIR spectrometer with 10-mm path length reduced-volume quartz cells (Starna Cells, Inc, Atascadero, CA). Transmission electron micrographs of nanoGUMBOS were obtained by a LVEM5 microscope (Delong America, Montreal, Canada) with an operating accelerating voltage of 5 kV. A JEOL model 100CX operating at an accelerating voltage of 80 kV was used to collect TEM micrographs of the gold seeds and gold-coated nanoGUMBOS. TEM samples were prepared on 400-mesh copper grids coated with an ultrathin carbon support film (Ted Pella, Redding, CA). Specimens were prepared by placing a 2 μL drop of solution onto the grid placed and allowed to dry at room temperature before analysis. SEM was performed using a SM-6610, JSM-6610LV high- and low-vacuum scanning electron microscope. Bare nanorods were sputter-coated with platinum under vacuum for 2 min to form a conductive layer necessary for imaging. This step was not required prior to imaging of gold-coated nanoGUMBOS.

Conclusions

In this work, we have synthesized and characterized thiol-functionalized nanoGUMBOS using both soft colloid and hard template routes. A reverse micellar nanoreactor approach afforded the ability to prepare very distinct nanoparticle sizes by varying the concentration of the reactants. At 1.0 M of aqueous-phase reactants, 21 nm nanoGUMBOS were formed and at a higher reactant concentration of 3.0 M, much larger 157 nm nanoGUMBOS were prepared. Gold-shelled nanoGUMBOS prepared from these materials demonstrated tunable optical properties which were highly dependent on the particle size and the ratio of gold hydroxide solution to gold-seeded particles used. Using an AAO template, rod-shaped nanoGUMBOS were formed. A similar gold coating route afforded gold-shelled nanorods displaying intense "panchromic" absorption with absorption spanning the entire visible and well into the NIR. These rod-shaped gold-shelled nanoGUMBOS also proved to be potent catalysts in the model reaction for reduction of 4-nitrophenol to 4-aminophenol using sodium borohydride.

To the best of our knowledge, this work represents the first example of a nanoscale *salt* being employed as a substrate to grow a gold-shelled core–shell functional nanomaterial. Given the wide scope for tailoring the chemistry, geometry, functionality, and morphology of nanoGUMBOS already demonstrated by us and others, coupled with clear similarities to gold-shelled silica materials, these results suggest intriguing potential and general scope for metal-shelled nanoGUMBOS in a host of areas, including catalysis, energy conversion, theranostics, and drug delivery.

Notes and References

[‡]Albemarle Corporation, Process Development Center, Baton Rouge, LA 70805.

[§]Aerospace Engineering, Texas A&M University, College Station, TX 77843.

[ǀ]Mechanical and Materials Engineering, Florida International University, Miami, FL 33174.

1   R. Chaudhuri, S. Paria, *Chemical Reviews,* 2012, **112**, 2373.
2   S.J. Oldenburg, R.D. Averitt, S.L. Westcott, N.J. Halas, *Chem. Phys. Lett.,* 1998, **288**, 243.
3   J.-H. Kim, H.-W. Chung, T.R. Lee, *Chem. Mater.,* 2006, **18**, 4115.
4   K/-T. Yong, Y. Sahoo, M.T. Swihart, P.N. Prasad, *Colloid Surf. A: Physicochem. and Eng. Aspects,* 2006, **290**, 89.
5   A.N. Bashkatov, E.A. Genina, V.I. Kochubey, V.V., Tuchin, *J. Phys. D: Appl. Phys.,* 2005, **38**, 2543.
6   X. Huang, P.K. Jain, I.H. El-Sayed, M.A. El-Sayed, *Photochem. Photobiol.,* 2006, **82**, 412.
7   X. Huang, P.K. Jain, I.H. El-Sayed, M.A. El-Sayed, *Lasers Med. Sci.,* 2008, **23**, 217.
8   L.R. Hirsch, R.J. Stafford, J.A. Bankson, S.R. Sershen, B. Rivera, R.E. Price, J.D. Hazle, N.J. Halas, J.L. West, *Proc. Natl. Acad. Sci. U.S.A.,* 2003, **100**, 13549.
9   D.P. O'Neal, L.R. Hirsch, N.J. Halas, J.D. Payne, J.L. West, *Cancer Lett.,* 2004, **209**, 171.
10   N.R. Jana, L. Gearheart, C.J. Murphy, *Adv.Mater.,* 2001, **13**, 1389.
11   X. Huang, S. Neretina, M.A. El-Sayed, *Adv. Mater.,* 2009, **21**, 4880.
12   A. Tesfai, B. El-Zahab, A.T. Kelley, M. Li, J.C. Garno, G. A. Baker, I.M. Warner, *ACS Nano,* 2009, **3**, 3244.
13   S. Das, D. Bwambok, B. El-Zahab, J. Monk, S.L. de Rooy, S. Challa, M. Li, F.R. Hung, G.A. Baker, I.M. Warner, *Langmuir,* 2010, **26**, 12867.
14   A.N. Jordan, S. Das, N. Siraj, S.L. de Rooy, M. Li, B. El-Zahab, L. Chandler, G.A. Baker, I.M. Warner, *Nanoscale,* 2012, **4**, 5031.
15   S.L. de Rooy, B. El-Zahab, M. Li, S. Das, E. Broering, L. Chandler, I.M. Warner, *Chem. Comm.,* 2011, **47**, 8916.
16   D.G. Duff, A. Baiker, P.P Edwards, *Langmuir*, 1993, **9**, 2301.
17   D.G. Duff, A. Baiker, I. Gameson, P.P. Edwards, *Langmuir*, 1993, **9**, 2310.

18 M.R. Rasch, K.V. Sokolov, B. A. Korgel, *Langmuir*, 2009, **25**, 11777.

19 N. Pradhan, A. Pal, T. Pal, *Langmuir*, 2001, **17**, 1800.

20 T. Premkumar, L. Kyungjae, K.E. Geckeler, *Nanoscale*, 2011, **3**, 1482.

21 M.H. Rashid, R.R. Bhattacharjee, A. Kotal,T.K. Mandal, *Langmuir*, 2006, **22**, 7141.

22 S. Wunder, F. Polzer, Y. Lu, Y. Mei, M. Ballauff, olyte Brushes. *J. Phys. Chem. C,* 2010, **114**, 8814.

23 E. Lam, S. Hrapovic, E. Majid, J.H. Chong, J.H.T. Luong, *Nanoscale*, 2012, **4**, 997.